Chaotic Oscillations of Tropical Climate: A Dynamic System Theory for ENSO

BIN WANG AND ZHENG FANG

Department of Meteorology, School of Ocean and Earth Science and Technology, University of Hawaii at Manoa, Honolulu, Hawaii

(Manuscript received 17 August 1995, in final form 26 February 1996)

ABSTRACT

Based on first principles, a theoretical model for El Niño–Southern Oscillation (ENSO) is derived that consists of prognostic equations for sea surface temperature (SST) and for thermocline variation. Considering only the largest-scale, equatorially symmetric, standing basin mode yields a minimum dynamic system that highlights the cyclic, chaotic, and season-dependent evolution of ENSO.

For a steady annual mean basic state, the dynamic system exhibits a unique limit cycle solution for a fairly restricted range of air–sea coupling. The limit cycle is a stable attractor and represents an intrinsic interannual oscillation of the coupled system. The deepening (rising) of the thermocline in the eastern (western) Pacific leads eastern Pacific warming by a small fraction of the cycle, which agrees well with observation and plays a critical role in sustaining the oscillation. When the nonlinear growth of SST anomalies reaches a critical amplitude, the delayed response of thermocline adjustment provides a negative feedback, turning over warming to cooling or vice versa.

When the basic state varies annually, the limit cycle develops a strange attractor and the interannual oscillation displays inherent deterministic chaos. On the other hand, the transition phase of the oscillation tends to frequently occur in boreal spring when the basic state is most unstable. The strongest boreal spring instability is due to the weakest mean upwelling and largest vertical temperature difference across the mixed layer base. The former minimizes the negative feedback of mean upwelling, whereas the latter maximizes the positive feedback of anomalous upwelling effects on SST; both favor spring instability. It is argued that the season-dependent coupled instability may be responsible for the tendencies of ENSO phase locking with season and period-locking to integer multiples of the annual period, which, in turn, create irregularities in oscillation period and amplitude.

1. Introduction

The Southern Oscillation implies an interannual mass exchange between the Eastern (Asian–Australian monsoon region) and Western (Pacific trade wind region) Hemispheres. Its physical cause had been a mystery for more than a half century until Bjerknes (1966, 1969) visualized a close association between atmospheric Walker circulation and SST contrast fluctuation in the equatorial Pacific Ocean. The equatorial SST contrast is primarily determined by the warming (El Niño) or cooling (La Niña) of the eastern Pacific cold tongue. The Southern Oscillation and the El Niño cycle, therefore, describe a unified interannual climate variation simply referred to as ENSO.

The complexity and nonlinearity of the ocean–atmosphere interaction pose great difficulties for theoreticians to explain ENSO using simple models. Consequently, numerical modeling became a popular approach. Successes have been achieved during the last decade in numerical simulation of ENSO with coupled intermediate models (e.g., McCreary and Anderson 1984; Cane and Zebiak 1985; Anderson and McCreary 1985; Zebiak and Cane 1987; Schopf and Saurez 1988), general circulation models (GCMs) (e.g., Philander et al. 1989; Latif et al. 1993), and hybrid models (Neelin 1989, 1990). The understanding gained from numerical experiments has considerably advanced our knowledge of ENSO physics.

At the same time, theoretical studies of the properties of the coupled ocean and atmosphere system have been extensively pursued, following Bjerknes' (1969) hypothesis. Neelin et al. (1994) provided a comprehensive review in this regard. Early theoretical analyses adopted prototype coupled models (McWilliams and Gent 1978; Lau 1981; McCreary 1983). Philander et al. (1984) presented the first rigorous stability analysis of a coupled shallow water system on an equatorial beta plane. Additional mechanisms and extensions were proposed in subsequent studies (e.g., Gill 1985; Yamagata 1985; Hirst 1986; Battisti and Hirst 1989; Xie et al. 1989; Neelin 1991; Wakata and Sarachik 1991; Jin and Neelin 1993a,b; Neelin and Jin 1993; Wang and Weisburg 1994). The development of a warm episode is now understood as resulting from a coupled instability of the atmosphere and ocean. Theoretical

Corresponding author address: Dr. Bin Wang, Dept. of Meteorology, School of Ocean and Earth Science and Technology, University of Hawaii, 2525 Correa Road, HIG 331, Honolulu, HI 96822. E-mail: bwang@soest.hawaii.edu

models developed thus far, however, are primarily confined to a linear dynamic framework and have made little progress in delineating nonlinear evolution of the coupled system.

Theoretical explanation of the temporal structure of the Southern Oscillation remains an outstanding challenge. A central question raised in Bjerknes' (1969) pioneering work was how the turnabout from a cold to a warm state takes place. Zebiak and Cane (1987) first attempted to address Bjerknes' puzzle by examining the cause of the oscillation in their numerical model. They found an increase of equatorial heat content prior to warm events and a sharp decrease during the events. The variability in the upper-ocean heat content was identified as a critical element of the model oscillation.

Primarily based on the perceptions gained from numerical experiments, Saurez and Schopf (1988) and Battisti and Hirst (1989) put forward a delay oscillator model for ENSO. Their semiempirical analog models highlighted how the coupled instability happens in the eastern Pacific and how the reflected equatorial waves at the western boundary provide a delayed, negative feedback to "shut down" the original growth. The delay that plays a central role in the above argument results from ocean wave dynamics as shown by Cane et al. (1990) and Schopf and Saurez (1990). The delay oscillator model demonstrates a certain degree of consistency with observed thermocline variability (Kessler 1991) and simulated large-scale baroclinic waves traversing an ocean basin in some ocean GCMs (Schneider et al. 1995) or coupled GCMs (Latif et al. 1993). However, the process involving reflection of Rossby waves at the western boundary is a matter of debate (Graham and White 1988; Battisti 1989; Chao and Philander 1993; Li and Clarke 1994; Mantua and Battisti 1994; Schneider et al. 1995). The basin-wide thermocline adjustment involves continuously forced, both locally and remotely, equatorial and off-equatorial waves propagating in the interior basin and reflected at meridional boundaries. Identification of precursors associated with reflected Rossby waves is extremely difficult.

In addition to the cyclic nature, ENSO exhibits at least two other prominent characteristics: irregularities in amplitude and frequency (Gu and Philander 1995; Wang and Wang 1996) and phase locking with annual cycles (Wyrtki 1975). Mature phases of warm episodes tend to occur in boreal winter (Rasmusson and Carpenter 1982). So do mature phases of cold episodes. The persistence of the Southern Oscillation breaks down during boreal spring (Trenberth and Shea 1987; Webster and Yang 1992). It has been suggested that ENSO irregularities might be the result of high-frequency stochastic forcing (e.g., Graham and White 1988; Mantua and Battisti 1995) or due to an inherent nonlinearity of the ENSO system (Vallis 1988; Munnich et al. 1991). Recent coupled intermediate numerical model experiments have demonstrated that the ENSO irregularities are essentially a low-order chaotic behavior driven by the annual cycle (Jin et al. 1994; Tziperman et al. 1994; Chang et al. 1994). The transition to chaos is featured by a tendency of frequency locking to $1/Q$ (year), where Q is an integer (Tziperman et al. 1995; Chang et al. 1995). The physical causes of the tendency for frequency-locking and the phase-locking to annual cycles, however, remain unclear.

Theoretical understanding of the essential physics of ENSO requires an analytical model. Any convincing theory that demonstrates new ideas must be derived from the first principles and based on adequate simplifications supported by observations. The theoretical model is also expected to be able to reproduce essential aspects of ENSO evolution: cyclic, chaotic, and phase-locking with annual cycles. Fundamental questions need to be addressed include

- Why does the climate of the coupled tropical ocean–atmosphere system oscillate in a highly irregular manner? Is the system inherent chaotic?
- Why does ENSO evolve with a tendency of phase-locking with annual cycle? In particular, why does warming often start and the persistence of the Southern Oscillation often break down in boreal spring?

The present study aims to address the above questions using a simple nonlinear ENSO model. We will, in section 2, derive a theoretical model from first principles. A number of simplifications are involved but none of them distorts essential physics of the coupled system. The spatial structure of ENSO allows for a crucial reduction of the three-dimensional model to a simple nonlinear dynamic system, which is capable of reproducing an irregular interannual oscillation that resembles ENSO. The model is instrumental for understanding the nature of the coupled mode, the mechanisms of the irregular oscillation, and the seasonal dependence of ENSO evolution.

2. Theoretical model for coupled tropical ocean–atmosphere

a. Governing equations

The ocean component of the coupled model is a simplified version of Zebiak and Cane (1987). The model consists of an active upper ocean with a mean depth H overlying an inert deep ocean. To better describe SST variation, the upper ocean above the thermocline is further divided into a well-mixed, frictional surface layer of constant depth (H_1) (hereafter referred to as mixed layer) and a subsurface layer (Cane 1979). To focus on ENSO physics, the model treats ENSO as a low-frequency departure from its climatological annual cycle. In the mixed-layer thermodynamic equation, meridional temperature advection will be neglected because 1) it plays a minor role and 2) its effect can be partially surrogated by vertical advection: convergence

of meridional currents tends to warm equatorial cold water, which is akin to an effect of anomalous downwelling. In the equatorial eastern Pacific where upwelling prevails nearly all the time, anomalous upwelling (or downwelling) could enhance (or suppress) mean upwelling and induce anomalous cooling (or warming). Further assume that all isotherms beneath the mixed layer move in harmony with the vertical thermocline displacement. A rise (deepening) of thermocline induces a decrease (increase) of the temperature of subsurface water upwelled into the mixed layer, T_e. A simple parameterization of T_e follows: $T_e(h) = \mu_*(\bar{h})h$ (Battisti and Hirst 1989), where the coefficient μ_* measures the degree of influence of thermocline fluctuation h on T_e. With the above considerations, the mixed-layer thermodynamic equation can be written as

$$\frac{\partial T}{\partial t} + \bar{u}_1 \frac{\partial T}{\partial x} + u_1 \frac{\partial}{\partial x}(T + \bar{T}) = -\frac{w}{H_1}(\bar{T} - \bar{T}_e + T - \mu_* h) - \frac{\bar{w}}{H_1}(T - \mu_* h) - \alpha_s T, \quad (2.1)$$

where T, u_1, and w denote anomalies of mixed layer temperature (hereafter refer to as SST), zonal currents, and the upwelling at the mixed layer base, respectively; overbars represent mean state quantities; α_s is a coefficient of Newtonian cooling that represents all processes that bring SST toward its climatology (Neelin et al. 1994).

Assume the motion is semigeostrophic (long-wave approximation). Further neglect the meridional wind stress in view of its minor role compared to zonal wind stress in the equatorial ocean. The equation governing thermocline displacement is (appendix A)

$$y^2 \frac{\partial h}{\partial t} + \frac{g'H}{\beta^2}\frac{\partial}{\partial t}\left(\frac{2}{y}\frac{\partial h}{\partial y} - \frac{\partial^2 h}{\partial y^2}\right) - \frac{g'H}{\beta}\frac{\partial h}{\partial x} = \frac{lU_a H}{\beta}\left(y\frac{\partial u_a}{\partial y} - u_a\right). \quad (2.2)$$

In the absence of wind forcing, Eq. (2.2) yields free equatorial Kelvin and long Rossby waves. These waves may be expressed in terms of generalized Laguerre functions (appendix B), which can be transformed to parabolic cylindrical functions used by Gill (1980) or Hermit polynomials used by Matsuno (1966). The equatorial mixed-layer zonal currents and the upwelling at the mixed layer base are, respectively, given by the following diagnostic equations [appendix A: (A.6) and (A.5)]:

$$u_1 = -\frac{g'}{\beta y}\frac{\partial h}{\partial y} + \frac{H_2}{H_1}\frac{lU_a\beta}{r_s}u_a, \quad (2.3)$$

$$w = -\frac{H_1}{H}\frac{\partial h}{\partial t} - H_2\frac{lU_a\beta}{r_s^2}u_a. \quad (2.4)$$

The second term in the rhs of (2.4) indicates that an equatorial anomalous westerly induces anomalous convergence and downwelling.

Surface winds are forced by SST gradients. A simplified Lindzen–Nigam (1987) model is adopted in which boundary layer winds are taken to be nondivergent [appendix A: (A.8a,b)]. This assumption is acceptable because the rotational zonal wind dominates its divergent counterpart even in the deep Tropics (Murakami and Wang 1993). The distortion of zonal winds owing to the above assumption is small over the equatorial wave guide where the ocean cares. With this simplification, it is easy to show that the zonal wind and the forcing in the rhs of (2.2) are

$$u_a = \frac{dR}{r_a^2 + \beta^2 y^2}\left(r_a\frac{\partial T}{\partial x} + \beta y\frac{\partial T}{\partial y}\right), \quad (2.5a)$$

$$\left(y\frac{\partial u_a}{\partial y} - u_a\right) = \frac{-dRr_a}{r_a^2 + \beta^2 y^2}\frac{\partial T}{\partial x} + f_1(T, y), \quad (2.5b)$$

where r_a is the Rayleigh frictional coefficient, d the atmospheric boundary layer depth normalized by the atmospheric density scale height, and R the gas constant, and

$$f_1(T, y) \equiv \frac{dRy}{r_a^2 + \beta^2 y^2}\left[r_a\frac{\partial^2 T}{\partial x \partial y} + \beta y\frac{\partial^2 T}{\partial y^2} - \frac{2\beta^2 y}{r_a^2 + \beta^2 y^2}\left(r_a\frac{\partial T}{\partial x} + \beta y\frac{\partial T}{\partial y}\right)\right]. \quad (2.5c)$$

Note that, $f_1(T, 0) \equiv 0$. Therefore, near the equator the principal wind forcing is simply proportional to zonal SST gradient.

The governing equations for the coupled ocean–atmosphere system have been reduced to two coupled prognostic equations: one for SST anomaly, Eq. (2.1), and the other for thermocline depth anomaly, Eq. (2.2). The SST and thermocline equations consist of a closed system with the diagnostic equation for mixed-layer zonal currents (2.3), upwelling (2.4), and zonal winds (2.5a,b). The essence of this theoretical model is the nonlinear coupling between mixed-layer thermodynamics and upper-ocean dynamics through wind stress and upwelling. The thermocline displacement plays a critical role, which not only "memorizes" effects of SST variation on winds but also conveys atmospheric feedback to SST in a nonlinear fashion via vertical temperature advection. The set of prognostic equations (2.1) and (2.2) will be referred to as the ENSO system.

b. Scale analysis

The model involves a number of basic parameters (listed in Table 1). Based on observations, we take

TABLE 1. List of the model parameters.

Geometrical parameters		
L	Zonal width of the ocean basin	1.7×10^7 m
H	Mean depth of the thermocline	150 m
H_1	Depth of the mixed layer	50 m
d	Nondimensional atmospheric boundary layer depth	0.2
Geophysical parameters		
β	Equatorial planetary vorticity gradient	2.28×10^{-11} m^{-1} s^{-1}
g'	Reduced gravity	2.8×10^{-2} m s^{-1}
$l = \rho_a C_D/\rho_0 H$	Wind stress coefficient	10^{-8} m^{-1}
Friction/damping parameters		
α_s	Newtonian cooling coefficient for SST anomaly	(125 day)$^{-1}$
r_s	Rayleigh friction coefficient in the oceanic mixed layer	(1.5 day)$^{-1}$
r_a	Rayleigh friction coefficient in the atmospheric boundary layer	3.6×10^{-6} s^{-1}
Other inherent parameters		
C_0	Oceanic Kelvin wave speed	2.0 m s^{-1}
L_0	Oceanic Rossby radius of deformation	300 km
$L_{rs} = r_s/\beta$	Ekman spreading length scale	338 km

one-half basin width $L/2$ and H_1 as characteristic zonal distance L_x and vertical thermocline displacement, respectively.

The characteristic scale for surface zonal wind speed, U_a, can be deduced from a primary balance between wind stress and pressure gradient force—the equatorial Sverdrup balance (Sverdrup 1947) [Eq. (A2b)]. Thus,

$$U_a = \left(\frac{g'H_1}{lL_x}\right)^{1/2}. \tag{2.6a}$$

Anomalous upwelling is primarily induced by Ekman pumping. Its characteristic scale can be estimated by the divergence of Ekman flows [Eq. (2.4)]. Thus,

$$W = \frac{\beta g'H_1H_2}{r_s^2 L_x}. \tag{2.6b}$$

The characteristic anomalous SST scale may be determined from the equatorial zonal momentum balance in the atmospheric boundary layer [Eq. (A.8a)]:

$$\theta = \frac{r_a}{dR}\left(\frac{L_x g'H_1}{l}\right)^{1/2}. \tag{2.6c}$$

The timescale relevant to ENSO development depends on the principal process that changes SST. The interannual variation of SST in the eastern Pacific results primarily from cooling (warming) associated with the anomalous upwelling (downwelling). This yields the ENSO development timescale:

$$\tau = \frac{r_s^2 L_x}{\beta g'H_2}; \tag{2.6d}$$

τ depends on r_s or the time interval required for oceanic Ekman flows to be fully adjusted to imposed wind forcing ($1/r_s$). If we take r_s equal to the intrinsic frequency scale $(\beta C_0)^{1/2} = O(10^{-5}\ \text{s}^{-1})$, then $\tau = HL_x/C_0H_2$, which represents a timescale for a Kelvin wave crossing the ocean basin. The ENSO development timescale, therefore, is the same order of magnitude as that for equatorial wave adjustment.

If the meridional scale of SST anomalies is set by meridional temperature advection associated with Ekman drift, one may estimate the SST meridional scale based on Ekman dynamics, which yields $L_{r_s} = r_s/\beta$ representing a meridional distance over which Ekman transport spreads SST anomalies on the ENSO development timescale. Again, if we take r_s equal to the intrinsic frequency scale $(\beta C_0)^{1/2} = O(10^{-5}\ \text{s}^{-1})$, the meridional SST scale is the oceanic Rossby radius deformation. Generally speaking, the characteristic meridional length scale for the coupled ENSO mode, L_y, should not be the oceanic Rossby radius of deformation because atmospheric wind response has a broader meridional scale, which results in a broader meridional scale for thermocline variation (this will in turn affect the time needed for thermocline adjustment). Without loss of generality, we treat L_y as a parameter that depends on the air–sea coupling coefficient. The reasoning is as follows: First, L_y is related to the characteristic zonal current scale U_0 as can be inferred from the semigeostrophic balance [Eq. (A.2c)]. Furthermore, when the westward acceleration produced by zonal wind stress is balanced by internal friction or entrainment across thermocline, the speed of the steady state zonal current is only a tiny fraction of the surface zonal wind speed due to the immense density difference between air and water. Assume the scale of zonal currents

$$U_0 = \alpha U_a, \tag{2.6e}$$

where α is an empirical air–sea coupling coefficient that measures the strength of ocean currents feedback per unit wind speed anomaly. Using (2.6e) and (A.2c) one can show that

$$L_y = L_0\left[\alpha^{-1/2}\left(\frac{H_1}{H}lL_x\right)^{1/4}\right], \tag{2.7}$$

where L_0 is the oceanic Rossby radius of deformation. The meridional length scale, therefore, depends on the air–sea coupling coefficient.

Using the parameter values listed in Table 1, we have $U_a = 4$ m s^{-1}, $W = 0.55$ m day^{-1}, $\theta = 2.1$°C, and $\tau = 3.05$ months. These characteristic scales agree reasonably well with observations.

It can be readily shown from (2.3) that the mixed-layer zonal currents associated with Ekman flows are substantially weaker than the vertical mean zonal currents because

$$\frac{O\left(\frac{H_2}{H_1}\frac{lU_a}{r_s}u_a\right)}{O\left(\frac{g'}{\beta y}\frac{\partial h'}{\partial y}\right)} = \frac{H_2}{H_1}\frac{L_y^2}{L_x L_{r_s}} \ll 1.$$

Here, we have assumed that $O(L_{r_s}) = O(L_y)$ and $L_y \ll L_x$. It can also be shown, from (2.4), that the upwelling at the mixed-layer base is predominantly driven by Ekman divergence because

$$\frac{O(\nabla\cdot\mathbf{V})}{O\left(\frac{H_2}{H_1}\nabla\cdot\mathbf{V}_e\right)} = \frac{H_1}{H}.$$

The expressions for w and u_1, (2.3) and (2.4), therefore, reduce to

$$u_1 = -\frac{g'}{\beta y}\frac{\partial h}{\partial y}, \tag{2.8}$$

$$w = -\frac{H_2 r \beta dR}{r_s^2 r_a}\frac{\partial T}{\partial x}. \tag{2.9}$$

Note that retaining the first term in (2.4) does not change the results qualitatively. Substituting (2.8) and (2.9) into (2.1) and using L_x, L_y, τ, θ, and H_1 to scale x, y, t, T, and h, respectively, one may obtain the following nondimensional SST and thermocline depth equations:

$$\frac{\partial T'}{\partial t'} = \frac{\partial T'}{\partial x'}\left(\Delta T_0' - \bar{u}_1' + T' - \mu' h' + \delta_1\frac{1}{y'}\frac{\partial h'}{\partial y'}\right) + \bar{T}_x'\left(T' - \mu' h' + \delta_1\frac{1}{y'}\frac{\partial h'}{\partial y'}\right) - \alpha_s' T' \tag{2.10a}$$

$$\delta\frac{\partial}{\partial t'}\left[y'^2 h' + \epsilon\left(\frac{2}{y'}\frac{\partial h'}{\partial y'} - \frac{\partial^2 h'}{\partial y'^2}\right)\right] - \frac{\partial h'}{\partial x'} = -\frac{\partial T'}{\partial x'}, \tag{2.10b}$$

where the prime denotes a nondimensional quantity, $\alpha_s' = \alpha_s\tau$, and the $f_1(T, y)$ in (2.5c) has been omitted as we focus on the oceanic wave guide in which $f_1(T, y)$ nearly vanishes. Inclusion of $f_1(T, y)$ requires tedious manipulation but does not alter the results qualitatively. The nondimensional basic state parameters in (2.10a,b) are

$$\Delta T_0' = (\bar{T} - \bar{T}_e)/\theta \tag{2.11a}$$

$$\bar{u}_1' = \bar{u}_1\tau/L_x \tag{2.11b}$$

$$\bar{T}_x' = \frac{L_x}{\theta}\frac{\partial \bar{T}}{\partial x}, \tag{2.11c}$$

where $\bar{T}_x'$ symbolizes zonal SST gradient or the strength of the mean upwelling [Eq. (2.9)]. The nondimensional numbers in (2.10a,b) are

$$\epsilon \equiv \frac{g'H}{\beta^2 L_y^4} = \left(\frac{L_0}{L_y}\right)^4 \tag{2.12}$$

$$\delta \equiv \frac{H_2}{H}\frac{\beta^2 L_y^2}{r_s^2} = \frac{H_2}{H}\left(\frac{L_y}{L_{r_s}}\right)^2 \tag{2.13}$$

$$\delta_1 = \frac{H_1}{H_2}\left(\frac{L_{r_s}}{L_y}\right)^2 = \frac{H_1}{H}(\delta)^{-1}. \tag{2.14}$$

All three nondimensional parameters depend on coupled meridional scale L_y or the air–sea coupling coefficient α. Parameter δ measures the importance of the non-Sverdrup balance, δ_1 represents the contribution of the horizontal temperature advection by anomalous zonal currents to local SST variation, and ϵ measures the relative importance of the equatorial wave motion to slow divergent motion associated with off-equatorial Rossby waves. Setting $\epsilon = 0$ corresponds to the neglect of local time change of zonal currents in Eq. (A.2b). That eliminates equatorially trapped waves.

There are two nondimensional coupling coefficients. One is the air–sea coupling coefficient α [Eq. (2.6e)] and the other is

$$\mu' = \frac{\mu_* H_1}{\theta}, \tag{2.15}$$

which measures the degree of coupling between thermocline and SST. For convenience, it will be referred to as the thermocline effect coefficient.

3. Dynamic system governing ENSO evolution

To focus on temporal behavior of the ENSO system, we apply the Lorenz (1963) method. In a zonally bounded yet meridionally infinite equatorial ocean basin, Cane and Moore (1981) showed, with the long-wave approximation, the existence of a free low-frequency standing wave mode that consists of long Kelvin and Rossby waves. Using a linearized version of the Zebiak and Cane (1987) model, Wakata and Sarachik (1991) demonstrated that the unstable coupled basin anomaly mode in a spatially varying basic state exhibits a similar structure. The thermocline variation in the western basin tends to be in an opposite phase with that in the eastern basin. These theoretical results are supported by observations. Wang (1996, manu-

script submitted to *Dyn. Atmos. Oceans*) has shown that the thermocline anomalies averaged over the western and over the eastern half of the Pacific basin between 15°N and 15°S (or between 25°N and 25°S) are nearly 180° out of phase. To the lowest approximation, the coupled basin mode may be treated as an equatorially trapped and symmetric east–west "seesaw".

The nondimensional meridional structure may thus be represented approximately by the lowest-order parabolic cylindrical function

$$D_0(y') = e^{-y'^2/2}. \tag{3.1}$$

Assume that the basic state is meridionally invariant (note that consideration of idealized meridional variation is solvable but involves complicated derivation). The solutions of the Eqs. (2.10a,b) can be approximately expressed by

$$T'_0 = \tilde{T}(x', t')D_0(y'), \tag{3.2a}$$

$$h' = \tilde{h}(x', t')D_0(y'). \tag{3.2b}$$

Substituting (3.2a,b) into (2.10a,b) and projecting the resultant equations onto $D_0(y')$ yields

$$\frac{\partial \tilde{T}}{\partial t'} = (\Delta T'_0 - \bar{u}'_1)\frac{\partial \tilde{T}}{\partial x'} + (\bar{T}'_x - \alpha'_s)\tilde{T} - (\mu' + \delta_1)\bar{T}'_x\tilde{h} + \sqrt{\frac{2}{3}}\frac{\partial \tilde{T}}{\partial x'}[\tilde{T} - (\mu' + \delta_1)\tilde{h}], \tag{3.3a}$$

$$\frac{\partial \tilde{h}}{\partial t'} = b\left(\frac{\partial \tilde{h}}{\partial x'} - \frac{\partial \tilde{T}}{\partial x'}\right) \tag{3.3b}$$

where

$$b \equiv \frac{2}{\delta(1 - 3\epsilon)} \tag{3.4}$$

is a nondimensional number that depends on the air–sea coupling coefficient (or L_y) and represents collective effects of all waves on slow thermocline adjustment. To the lowest order, we treat ENSO as a basin standing mode with one pole in the eastern Pacific ($x'_E = 0.5$ representing 120°W) and the other in the western Pacific ($x'_W = -0.5$ denoting 160°E). Consistent with observations and for simplicity, we assume that the SST anomaly vanishes at x'_W and its amplitude increases eastward linearly, so that $\partial \tilde{T}/\partial x' = T_E$, where T_E denotes SST anomaly at x'_E. Assume the node point of the standing thermocline oscillation is located at the middle of the basin, $x'_0 = 0$. The thermocline displacement in the eastern basin can be solved with a boundary condition $h'(x'_0) = 0$. The anomalous SST and thermocline depth at the eastern Pacific, T_E and h_E, are therefore governed by

$$\frac{dT_E}{dt} = a_1T_E - a_2h_E + \sqrt{\frac{2}{3}}\,T_E(T_E - a_3h_E) \tag{3.5a}$$

$$\frac{dh_E}{dt} = b(2h_E - T_E), \tag{3.5b}$$

where

$$a_1 = (\Delta T'_0 - \bar{u}'_1 + \bar{T}'_x - \alpha'_s)|_{x_E} \tag{3.6a}$$

$$a_2 = (\mu + \delta_1)\bar{T}'_x|_{x_E} \tag{3.6b}$$

$$a_3 = (\mu + \delta_1), \tag{3.6c}$$

and $\mu = \mu'|_{x_E}$.

The dynamic system (3.5a,b) describes the interannual variation of the coupled system in the core region of ENSO: SST and thermocline variations in the Niño-3 region and wind anomaly over the central Pacific. The evolution of ENSO is governed by a nonlinear dynamic system that is second order in time with time-dependent coefficients, differing from the delay oscillator model.

4. Solutions

a. Equilibrium states, coupled instability, and linear behavior

The ENSO dynamic system, (3.5a,b), possesses two steady solutions:

$$T_E^{(1)} = h_E^{(1)} = 0, \tag{4.1a}$$

$$T_E^{(2)} = 2h_E^{(2)} = \frac{2a_1 - a_2}{2a_3 - a_4}. \tag{4.1b}$$

The first steady solution is the origin in the phase space and represents the climatological mean equilibrium state or an ENSO "transitional" state in which both SST and h are normal. The model's climatological mean states (annual cycles) are illustrated in Fig. 1. They were obtained by running an intermediate tropical Pacific Ocean model (Wang et al. 1995) using observed climatological monthly mean solar radiation, surface wind stress, and cloudiness forcing.

The climatological equilibrium state becomes unstable when $a_1 + 2b > 0$ (the primary bifurcation). The corresponding perturbation growth rate

$$\gamma = \frac{1}{2}(\Delta T'_0 - \bar{u}'_1 + \bar{T}'_x - \alpha'_s)|_{x_E} + \frac{2}{\delta(1 - 3\epsilon)} \tag{4.2}$$

depends on climatological mean state and the air–sea coupling coefficient α, but not the thermocline effect coefficient μ. For a given mean state, the growth rate increases exponentially with increasing coupling coefficient α or decreasing meridional scale of the coupled mode (Fig. 2a). For a given α, the growth rate varies with season. The largest (smallest) growth occurs for a boreal spring (fall) mean state. Additional computations reveal that the annual change of the coupled stability is mainly caused by annual variation of

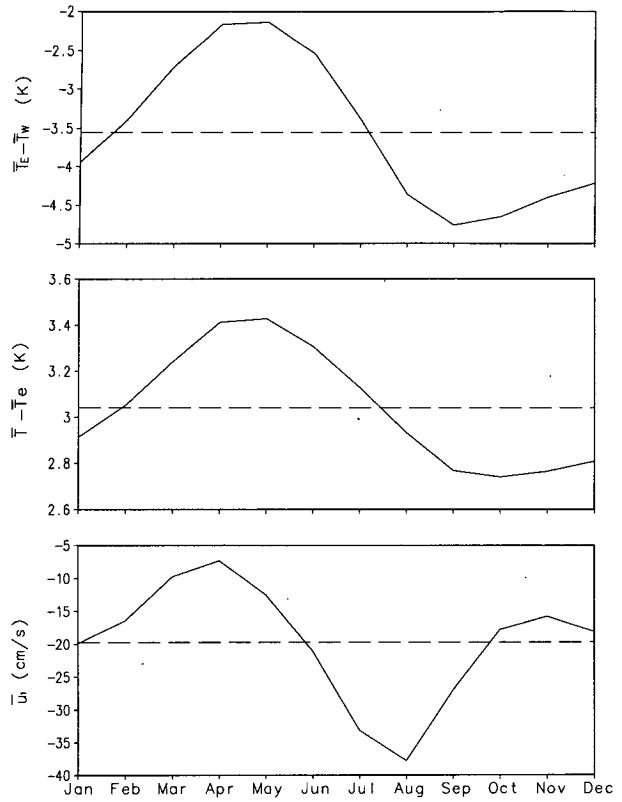

FIG. 1. Climatological mean annual cycles used in the model: (a) SST difference between equatorial eastern ($\bar{T}_E$) and western ($\bar{T}_W$) Pacific; (b) the temperature difference between the mixed-layer and subsurface-layer water, $\bar{T} - \bar{T}_E$; and (c) the mean equatorial zonal currents $\bar{u}_1$ averaged over Niño-3 region.

zonal SST gradients or mean upwelling and the temperature difference across the mixed layer base.

Perturbations in the vicinity of the climatological equilibrium state may approach (or depart from) it either asymptotically or oscillatorilly. It is readily shown that the presence of a linear oscillatory solution (growing or damping oscillation) requires

$$0 < \frac{a_1 - a_2}{2} - \frac{1}{2}(a_2^2 - 2a_1a_2)^{1/2} < b < \frac{a_1 - a_2}{2} + \frac{1}{2}(a_2^2 - 2a_1a_2)^{1/2} \quad (4.3)$$

and

$$\mu > -\delta_1 + \frac{2}{\bar{T}'_x}(\Delta T'_0 - \bar{u}'_1 + \bar{T}'_x - \alpha'_s). \quad (4.4)$$

The oscillatory behavior occurs only when b, and therefore α, takes restrictive positive values and μ exceeds a threshold. The linear oscillation period is

$$\tau^* = 4\pi\tau[4b(a_1 - a_2 - b) - a_1^2]^{-1/2}, \quad (4.5)$$

which depends on basic climatic state, α, μ, and model's geophysical parameters. For given parameters listed in Table 1, the oscillation period τ^* is an order of magnitude longer than the ENSO development timescale τ. It decreases with increasing μ but depends on α in a subtle manner: The longest oscillation period occurs for an intermediate air–sea coupling strength (Fig. 2b). When the vertical temperature gradient ($\Delta T'_0$) decreases, oscillation requires a considerably larger μ; meanwhile, the oscillation period lengthens (Fig. 3a). The oscillatory behavior also sensitively depends on the mixed-layer friction, r_s (Fig. 3b). Decreasing r_s markedly raises the threshold μ and increases the oscillation period.

The second equilibrium state, (4.1b), is located on the straight line $T_E - 2h_E = 0$ and represents an unstable saddle point in the phase space. It is physically triv-

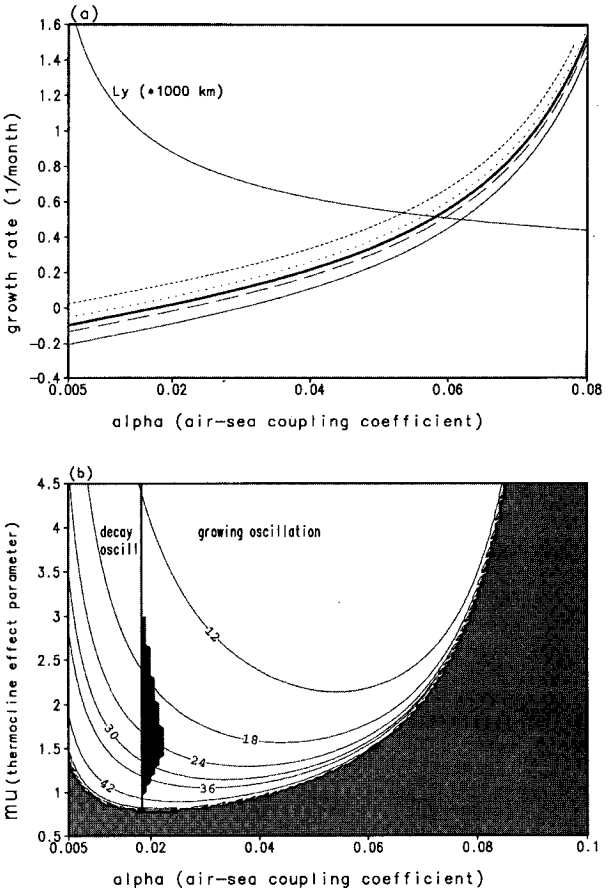

FIG. 2. Linear behavior of the ENSO dynamic system: (a) the growth rate as a function of α for the annual mean (thick solid line), January (long dashed line), April (short dashed line), July (dotted line), and October (thin solid line) basic state; and (b) the oscillation period (month) as a function of α and μ for annual mean basic state. The light shading represents the nonoscillatory domain; the dark shading outlines the domain of nonlinear oscillation (limit cycle). Also given in (a) is the meridional length scale L_y as a function of α.

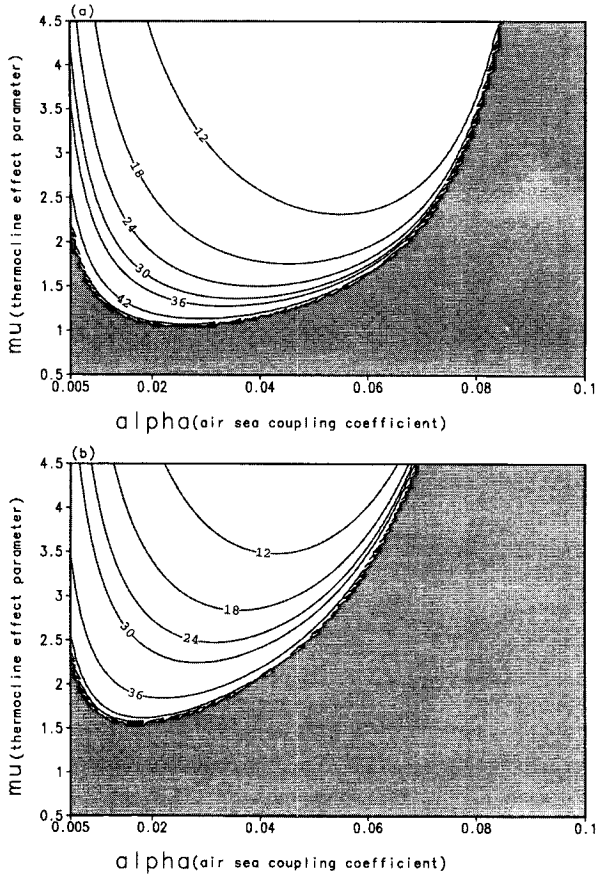

FIG. 3. The convention is the same as in Fig. 2b except that (a) shows the influence of $\Delta\bar{T}_0$ (temperature difference between the mixed-layer and subsurface-layer water), which was changed from 3.0° to 2.5°C, and (b) shows the effect of Rayleigh friction coefficient in the mixed layer r_s, which was changed from 1.5 to 1.0 day^{-1}.

ial. For typical mean state parameters this steady solution is also unrealistic.

b. *Limit cycle solution for the annual mean basic state*

For the ENSO dynamic system (3.5a,b), we are more interested in finding out whether finite-amplitude, periodic solutions (or limit cycles) exist. We first examine the case in which the basic state is time independent (the annual mean state shown in Fig. 1). In this case, the dynamic system is a second-order autonomous system with one focus and one saddle point when $\mu > \mu_0$. Such a system can have at most one limit cycle solution. Furthermore, if a limit cycle exists it must encircle only the focal point (the climatological mean state). Since the ENSO dynamic system contains two coupling coefficients as parameters, it is important to find the parameter domain in which the limit cycle solution may exist.

Appendix C shows that for a given steady basic state the ENSO dynamic system possesses one and only one limit cycle solution if conditions (C.6) and (C.7) are satisfied. Figure 4 illustrates the parameter domains in which the condition (C.6) is valid and the values of d defined by (C.7) are sufficiently small, providing a guidance for numerical search for limit cycle solutions in the parameter space. The actual parameter domain in which limit cycle exists (shown by the dark shading area in Fig. 4) was determined by numerical integration of (3.5a,b). The numerical results suggest that (C.6) and (C.7) are necessary conditions for the existence of a limit cycle.

The limit cycle territory is imbedded in a spacious domain of linear oscillation (Fig. 2b), indicating it exists only in a restricted range of the air–sea coupling coefficient. This implies that search for oscillation in coupled numerical models is often a challenging task. Note also that the limit cycle occurs at the primary bifurcation point, indicating the first bifurcation is a Hopf bifurcation. This agrees with Neelin's (1990) assertion.

In the phase plane, the limit cycle is an elliptic encircling the climatological equilibrium state (Fig. 5a). The second equilibrium state, being a saddle point, is necessarily located outside the limit cycle. Numerical experiments further demonstrate that the limit cycle is a stable attractor. Any perturbed initial state starting from inside the limit cycle or from outside but within a realistic distance (restricted by the location of the unstable saddle point) will eventually be attracted to the limit cycle.

In the physical space, the limit cycle represents a perpetual, finite-amplitude oscillation as shown in Fig. 5b. Note that the thermocline displacement slightly leads SST variation. The cycle is asymmetric: warming takes much longer than cooling. Further studies indi-

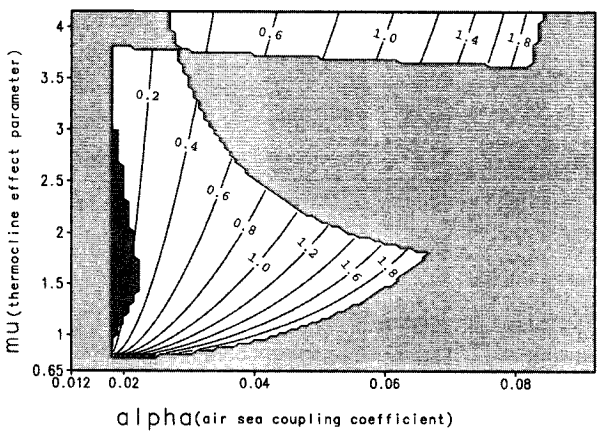

FIG. 4. Search for the domain of existence for the limit cycle in parameter space. The contour shows values of d (C.7) in the area where condition (C.6) meets. The dark shading indicates the domain of existence for the limit cycle determined by numerical integrations.

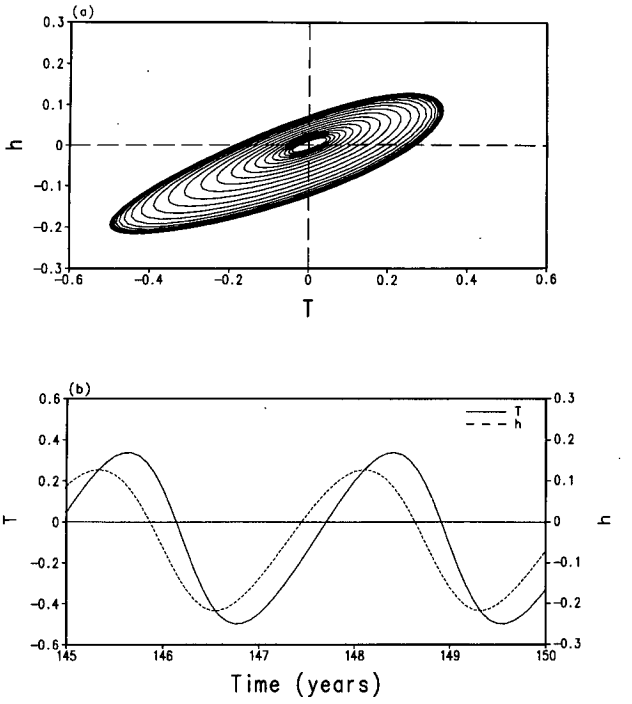

FIG. 5. The limit cycle solution for annual mean basic state and $\mu = 1.315$, $\alpha = 0.0184$. (a) The phase orbit. When $\alpha > \alpha_0$ the perturbation initially located near the origin (the annual mean state) grows and oscillates, approaching the limit cycle. (b) Time series of anomalous SST (solid line) and thermocline depth (dashed line) from model integration year 145 to year 150.

cate that the degree of asymmetry varies with the strength of the nonlinearity.

The period and amplitude of the model's nonlinear oscillation depend on the climatological mean state and the coupling coefficients. Figure 6a displays the period as a function of μ and α for the given annual mean state shown in Fig. 1. For typical parameter values listed in Table 1, the oscillation period ranges from 18 to 60 months. Note that the oscillation period is primarily determined by the parameter μ, suggesting the importance of the effect of thermocline displacement on SST in setting up the oscillation timescale. Note also that the period calculated for linear oscillation near the climatological equilibrium state provides a good estimate for the nonlinear oscillation (Figs. 2 and 6a), suggesting the usefulness of the linear analysis (Figs. 3a,b for instance). The amplitude of nonlinear oscillation is also in a reasonable range for the given annual mean basic state (Fig. 6b). As μ and α increase, amplitude increases at a comparable rate.

c. *Strange attractor in the presence of the basic-state annual cycle*

With a time-independent basic state, the ENSO dynamic system can have only regular nonlinear oscillation: chaos does not exist in a second-order autonomous system. When the basic state includes an annual cycle, however, the ENSO system becomes nonautonomous and increases its degrees of freedom, thereby possibly entering a chaotic regime when the amplitude of the basic-state annual cycle exceeds a threshold value. This is indeed the case when the annual cycles shown in Fig. 1 are taken as a basic state.

Figure 7a shows the phase orbit of the irregular oscillation of the dynamic system with the annual cycle basic state. The parameters used in Fig. 7a are identical to those used in Fig. 5a except for the basic state. The chaotic phase orbits in Fig. 7a are trapped in the vicinity of the limit cycle shown in Fig. 5a, indicating that the limit cycle becomes a strange attractor when the basic state varies annually.

The corresponding power spectra for the above regular and chaotic oscillations are compared in Fig. 7b. For the regular oscillation (the limit cycle), the primary energy peak appears on an oscillation period of about

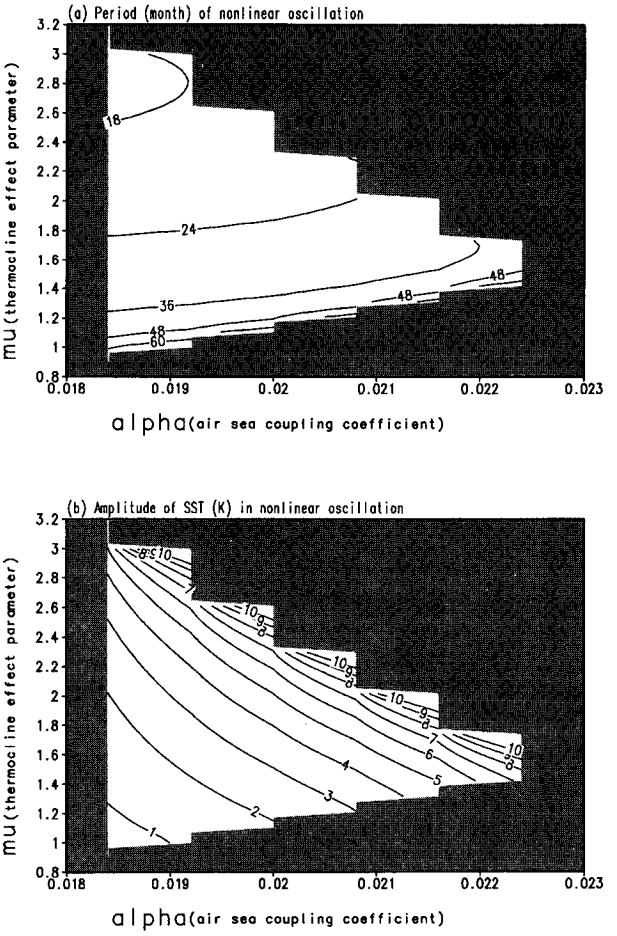

FIG. 6. Dependence of (a) the period (month) and (b) the amplitude (°C) of SST anomaly of the limit cycle on α and μ for the annual mean basic state.

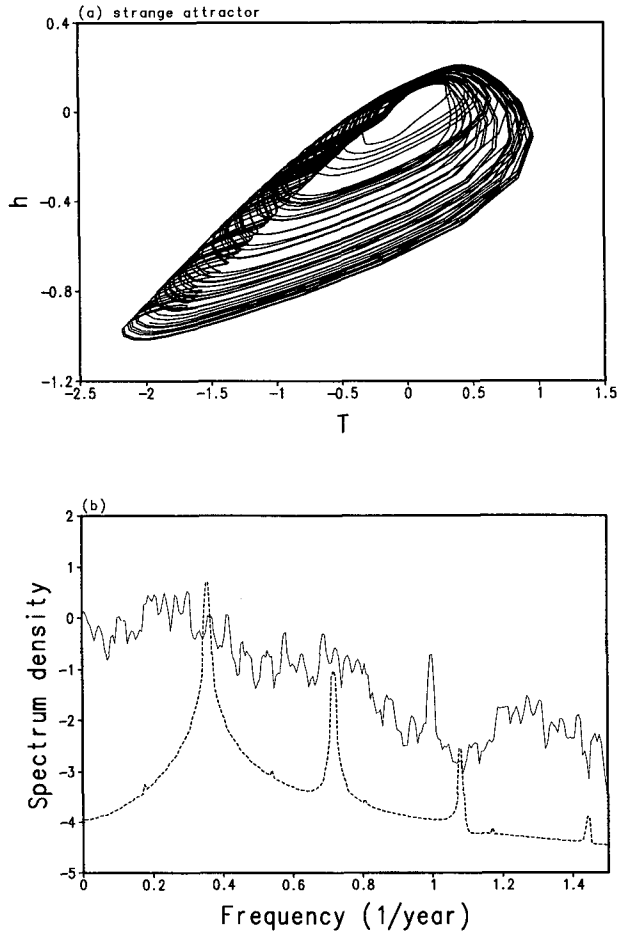

FIG. 7. The chaotic oscillation for the annual cycle basic state and $\mu = 1.315$, $\alpha = 0.0184$. (a) Phase portraits of the strange attraction to the limit cycle. (b) Log spectrum density of SST anomaly (solid). In (b) the dashed curve is derived for the limit cycle solution shown in Fig. 5.

34 months; the secondly subharmonic peaks result from the asymmetric evolution of the limit cycle. The existence of chaos broadens and smears the primary energy peak and shifts it to lower frequency. It is interesting to notice the sharp peak on the annual timescale, which manifests the influence of the annual variation of the basic state on the ENSO mode. This resonant response also means a possible rectification of the annual cycle of basic state by the chaotic ENSO oscillation.

5. Relevance of the model oscillation to ENSO

The limit cycle describes model's intrinsic oscillation. To demonstrate its relevance to ENSO, we show an observed anomalous SST-h scattering diagram for the period of July 1982 to November 1986, roughly one cycle (Fig. 8a). The depth of the 20°C isotherm was used as a surrogate for the thermocline depth. The theoretical limit cycle orbit shown in Fig. 5a matches the observed phase loop (Fig. 8a) qualitatively.

The temporal structure of the model oscillation in SST and h also bears similarities with the observed ENSO cycles from June 1982 to December 1992 (Fig. 8b). First, the phase of anomalous thermocline depth leads that of the SST anomaly by a small fractional cycle in both the model (Fig. 5b) and the observation (Fig. 8b). Second, the rise of SST takes longer than the ensuing collapse (Figs. 5b and 8b). The interannual oscillation that appeared in the coupled GCMs of Philander et al. (1992) exhibits similar features. In various versions of Zebiak and Cane's models (Battisti and Hirst 1989; Chang et al. 1994) and the hybrid coupled model (Neelin 1990), the interannual oscillations obtained for steady basic states are essentially limit cycle-type of solutions.

In the eastern tropical Pacific, most El Niño episodes tend to start during the warm season and mature near the end of the year. The persistence of the Southern Oscillation also breaks down during the warm season of the cold tongue. In the present model, when the basic state varies annually, the warming most frequently starts in late boreal spring (May) (Fig. 9a) and peaks in late boreal winter (February) (Fig. 9b). This resembles the observed ENSO phase-locking to annual cycle. The model thermocline oscillation is also phase-

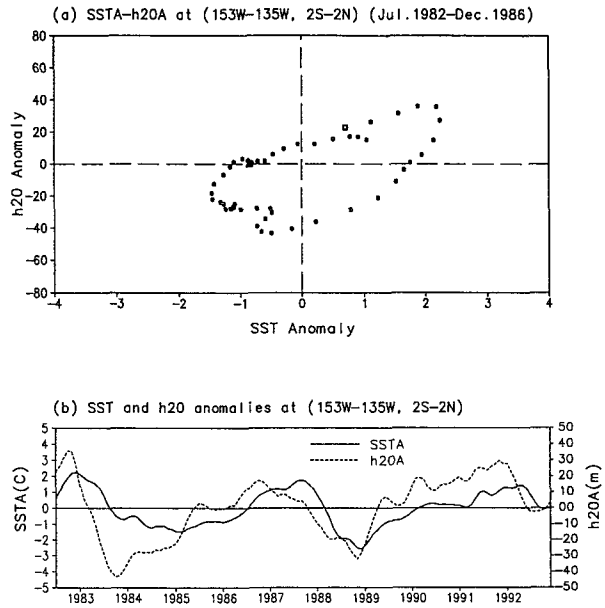

FIG. 8. Observed anomalous monthly mean SST (°C) and depth of 20°C isotherm (m) derived from NCEP ocean reanalysis (Ji et al. 1995) for the equatorial eastern Pacific (2°S–2°N, 153°–135°W) region: (a) Scattering diagram for the period of July 1982 to December 1986, roughly one ENSO cycle. Each closed dot denotes one calendar month. The square denotes the beginning month. (b) Reconstructed time series for the period of July 1982–December 1992. Only the first two EOF modes are used for the reconstruction.

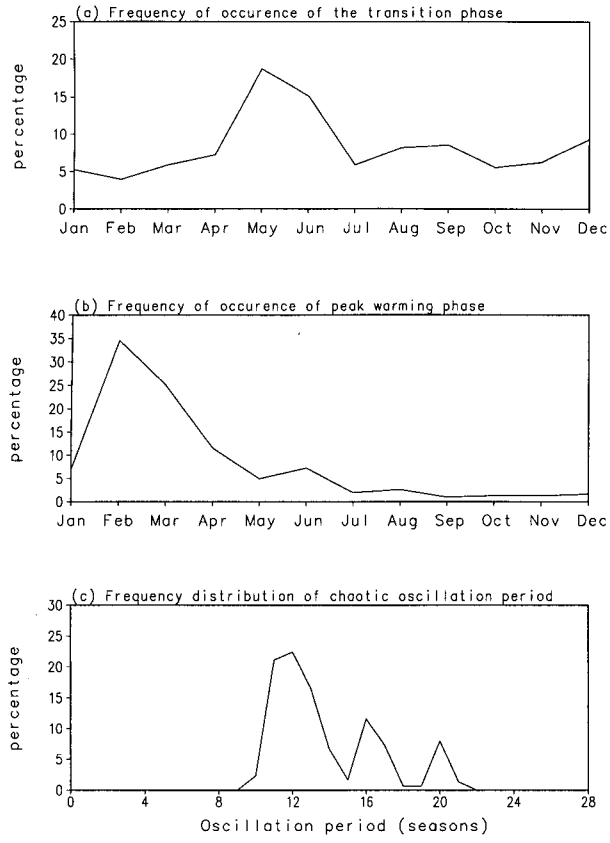

FIG. 9. The phase-locking and frequency-entrainment in the chaotic oscillation for the annual cycle basic state and $\mu = 1.315, \alpha = 0.0184$. (a) Frequency of occurrence (percentage) of the transitional phase in each calendar month. (b) As in (a) except for the peak warming phase. (c) Frequency distribution of the oscillation period measured by the time interval between two adjacent peak warmings (in units of season).

locked with the basic-state annual cycle but the preferred transition phase is 3 months ahead of SST transition—in boreal winter (figure not shown), indicating that the basic state annual cycle does not alter the phase relationship between thermocline displacement and SST.

The favorable comparisons add confidence to the relevance of the model oscillation to ENSO cycles and to the interannual oscillations found in the coupled numerical models. It suggests that the ENSO dynamic system captures the basic oscillatory nature of the observed ENSO cycle.

6. Mechanism of the model oscillation

For a restricted range of the air–sea coupling coefficient, the model produces interannual oscillations. A number of questions need to be addressed here. First, which process(es) is(are) essential for the oscillation? Second, how does a warming change to a cooling or vice versa?

The first question is easy to answer because the oscillation is essentially nonlinear while the model's nonlinearities are contained only in the ocean thermodynamics. The temperature advection must be essential for the model's finite amplitude oscillation. As seen from Eqs. (3.6b,c), the effects of horizontal temperature advection signified by δ_1 play the same roles as those of the thermocline fluctuation on vertical temperature advection signified by μ. Quantitatively, however, the vertical advection makes a greater contribution.

The model oscillation is sustained by the nonlinear interaction between SST and thermocline variations. The thermocline variations directly influence SST via changing the upwelled water temperature. This is a "fast" process, taking only a small fraction of the oscillation period (a few months). It is this process that sets up the phase of thermocline variation leading that of SST variation in the eastern Pacific. The SST variation, on the other hand, indirectly affects thermocline variation through changing wind stress. This is a "slow" adjustment processes, taking the major portion of the oscillation period.

The slow adjustment process may be alluded from Eq. (2.10b), which describes how SST gradients (wind stresses) force upper ocean and change thermocline depth. In general, the zonal wind stress and pressure gradient force associated with thermocline slope are not in equilibrium balance. In fact, the nondimensional parameter δ is an $O(1)$ quantity [see (2.13)]. The imbalance between wind stress and thermocline variation excites two forms of motion: fast equatorial Kelvin and Rossby waves and slow divergent flow associated with the off-equatorial quasigeostrophic Rossby waves. The relative contribution of the two components is symbolized by parameter ϵ [Eq. (2.12)]. Setting $\epsilon = 0$ eliminates equatorially trapped waves. In this limit, however, there remains slow divergent motion forced by wind stress and deflected by the Corriolis force, which can result in a slow thermocline adjustment. It would be interesting to perform a distorted-physics experiment in which ϵ vanishes and to examine the thermocline adjustment. The observed equatorial thermocline displacement appears to involve fast Kelvin wave passages (free waves in the eastern Pacific) on intraseasonal timescale and a slow eastward propagation of a wave packet (coupled with zonal wind anomalies) on interannual timescale. It seems plausible to suggest that the former manifests fast wave adjustment whereas the latter reflects slow adjustment associated with the coupled basinwide mode.

In reality, the slow basin-wide thermocline adjustment is a complex process that involves both equatorial and off-equatorial (forced and free) waves propagating and reflecting in the bounded basin. The slow thermocline adjustment can be viewed as a delayed response to the change of SST in the eastern equatorial Pacific. The present dynamic system model does not

deny essential roles of the wave dynamics in this delayed response, rather, it takes into account the collective wave effects by simply assuming the coupled basin mode being a standing seesaw resulting from the superposition of numerous equatorial and off-equatorial waves generated by local or remote wind forcing associated with SST variation and reflected from two meridional boundaries. This bypasses the difficulty to directly deal with complex wave adjustment process and leads to a maximum simplification of the ENSO system (2.10a,b). In this way, the delayed adjustment is built in the standing seesaw assumption. We emphasize that the delayed adjustment is a behavior of the coupled basin mode and takes a much longer timescale than that of equatorial wave crossing the basin.

In essence, the delayed oscillator model does not need to consider detailed mixed-layer thermodynamic processes. It can be derived by an instantaneous equilibrium balance between SST and thermocline variation in the eastern Pacific (Cane et al. 1990). Different from this thermodynamic equilibrium point of view, the present model emphasizes the essential role of the phase leading of thermocline to SST variation in the eastern Pacific in sustaining the oscillation. This is equivalent to emphasizing the roles of the mixed layer thermodynamics and slow SST mode alluded to by Neelin (1991). Figure 10 explains this point. The system (3.5a,b) has two characteristic lines given by $dT_E/dt = 0$ and $dh_E/dt = 0$, which are, respectively,

$$h = T\frac{a_1 + a_3T}{a_2 + a_4T} \equiv f(T) \tag{6.1}$$

$$h = \frac{T}{2}. \tag{6.2}$$

The two characteristic lines divide the limit cycle into four phases (Fig. 10). During the phase I (and III), SST and h have the same tendency: the deepening (or shallowing) of thermocline and rising (or lowering) of SST occur simultaneously. The phase leading of thermocline variation, however, plays a critical role in switching over from one state to another. It yields an opposite tendency in thermocline and SST variations during the phase II (and IV). Thus, the shoaling of thermocline eventually stops the increase of SST (in phase II) or vice versa (in phase IV). It is the phase lead between the thermocline and SST variations that provides a negative feedback turning the coupled system from a warming or cooling to an opposing process.

Therefore, in the present model, both the upper-ocean dynamics (delayed thermocline response to SST variation) and the mixed-layer thermodynamics (phase lead of thermocline to SST variation) are essential elements for the coupled oscillation mode. This mode is characterized by a nonlinear interaction between slow upper-ocean divergent motion and SST variations, which is realized through air–sea coupling (surface wind stress and upwelling) in a spatially and temporally varying basic state. The model emphasizes not only the importance of the slow thermocline displacement–SST interaction, but also the fundamental impacts of the basic state variations on air–sea coupling, as will be discussed in the next section.

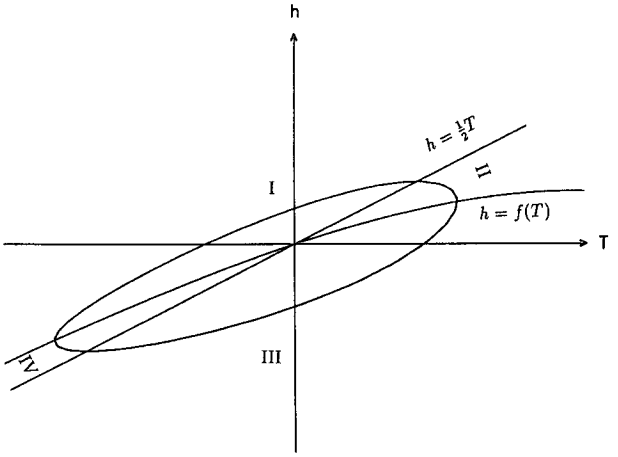

Phase	$\frac{dT}{dt}$	$\frac{dh}{dt}$
I	+	+
II	+	−
III	−	−
IV	−	+

FIG. 10. Schematic diagram showing the phases of the nonlinear oscillation. The limit cycle is the same as in Fig. 5a.

7. Impacts of the annual cycle

Solutions shown in Figs. 7 and 9 indicate that the annual basic state plays dual roles in ENSO cycle. On the one hand, it generates deterministic chaos; on the other hand, it regulates ENSO evolution, causing occurrence of transition (or mature) phase of ENSO in a fixed season on a regular basis. This agrees very well with the results obtained from coupled intermediate numerical model experiments performed by Chang et al. (1995) and Tziperman et al. (1995).

The phase-locking of the model's interannual oscillation with annual cycle may be partially due to seasonal dependence of the coupled instability of the basic state. Figure 2a shows that the climatological basic state is most unstable (stable) in boreal spring (fall). For the nonlinear oscillation, which requires $\alpha < 0.03$ (Fig. 2b), perturbations amplify in boreal spring basic state, whereas they decay in boreal fall and winter basic state. The implication is that boreal spring may be the season during which ENSO has weakest persistence and development of warming is favored due to potential fast growth of perturbations, whereas the boreal fall and subsequent winter basic states would tend to level off the ongoing growth and favor maturation of warm-

ing. We have tested this idea by shifting the phase of annual cycle forward by 6 months: The northern fall becomes the most unstable season. The corresponding warming then tends to start in November and peak in the late northern summer, indicating the ENSO phase lock is indeed controlled by annual variation of the basic-state instability.

Hypotheses regarding the cause of the preferred boreal spring coupled instability have been proposed. Philander (1990) conjectured that the initiation of unstable ocean–atmosphere interactions requires that unusually warm surface waters cause a local heating of the atmosphere; therefore, the coupled system is more unstable in boreal spring than boreal autumn. Others postulated that the boreal spring is the season during which ocean–atmosphere coupling is weakest. The weakest coupling invites random growth of perturbations. The latter may cause loss of predictability. In the present model, the frequent initiation of ENSO warming in boreal spring is not due to the weak coupling between the ocean and atmosphere (because the coupling coefficient is invariant), rather, it is due to a strong coupled instability: The largest vertical temperature difference $(\bar{T} - \bar{T}_e)$ and the weakest east–west thermal contrast $\bar{T}_x'$ (as well as the weakest easterly wind stress and equatorial upwelling) during boreal spring is most favorable for coupled perturbations to grow. The reasons follow: Suppose SST is initially higher than normal. First, the initial warming would induce an anomalous westerly and downwelling, which acts on mean vertical temperature gradient $(\bar{T} - \bar{T}_e)$, further enhancing warming. Increase of $(\bar{T} - \bar{T}_e)$ during boreal spring reinforces this positive feedback and favors coupled instability. Second, the initial warming would also increase the anomalous vertical temperature gradient, which enhances cooling associated with mean upwelling and suppresses initial warming. However, the weak mean upwelling in boreal spring would minimize this negative feedback, also favoring spring coupled instability.

The preferred transition of the ENSO cycle in boreal spring implies a weak spring persistence of the Southern Oscillation index. It may contribute to the spring prediction barrier of SST anomalies. Using an intermediate ocean model coupled to a statistical atmosphere, Balmaseda et al. (1995) found that their model's heat content has a prediction barrier in boreal winter. The preferred thermocline transition in boreal winter demonstrated in the present model may explain the loss of predictability of model heat content in boreal winter.

As a result of the tendency of mature phase locking to annual cycle, the oscillation period counted by the intervals between two adjacent peak warmings tends to be an integer multiple of the annual period. Figure 9c clearly illustrates such a tendency. For an annual mean basic state, the system has an intrinsic oscillation period of about 34 months. The annual variation of the basic state not only develops irregularity in oscillation period but also tends to "lock" the period to 3, 4, and 5 years. Changes in oscillation period are expected to create irregularities in the oscillation amplitude.

Physically, the seemingly opposing effects of the annual cycle—generation of chaos shown by the strange attractor in Fig. 7a and the phase and period regulation shown in Figs. 9a–c—may actually have the same origin: the modulation of the intrinsic coupled oscillation by the annual cycle through seasonally varying coupled instability of the basic state. The season-dependent coupled instability causes ENSO phase-locking to annual cycle, and thus a period-locking to the integer multiple of annual period, which, in turn, results in irregularities in the period and amplitude of the oscillation.

Our extensive numerical experiments show that the route leading to chaos is through period doubling, and the period tends to lock to integer number of years in a similar way as shown in numerical experiments of Chang et al. (1995).

8. Summary

A theoretical model for the coupled tropical ocean and atmosphere is derived from a coupled Zebiak and Cane's (1987) ocean and Lindzen and Nigam's (1987) atmospheric model. We show that the essential physics of the coupled system can be described by a so-called ENSO system, which consists of two prognostic equations, one for SST and the other for thermocline variation. The ENSO system (2.10a,b) provides a useful theoretical framework for study of interannual variation of the tropical climate system.

The observed ENSO can be approximately considered as an equatorially symmetric east–west standing oscillation. This standing oscillation mode can be viewed as the free eigenmode (Cane and Moore 1981) or coupled unstable basin mode (Wakata and Sarachik 1991) in the meridionally bounded Pacific basin. Considering only the largest-scale, standing basin mode, we show that the evolution of ENSO is depicted by a minimum dynamic system (Lorenz 1963)—a set of second-order nonlinear ordinary differential equations with coefficients varying periodically with time.

The system has an equilibrium state—the climatological mean basic state—which may become unstable as the air–sea coupling coefficient exceeds a critical value. The mean state is most unstable (stable) in northern spring (fall) because the weakest mean upwelling minimizes its negative feedback to SST and the largest vertical temperature gradient across the mixed-layer base maximizes the positive feedback of anomalous upwelling to SST; both favor coupled instability in boreal spring. The rate of perturbation growth depends on the air–sea coupling coefficient, whereas the way by which perturbations grow (oscillatorilly or asymptotically) is determined by both the air–sea cou-

pling and the thermocline effect coefficients. The coupled instability is mainly affected by the strength of the mean upwelling or the east–west SST gradient, while the oscillatory behavior is more sensitive to the vertical temperature gradient across the mixed-layer base.

When the basic state is the climatological annual mean, the ENSO dynamic system is autonomous. For a fairly restricted range of the air–sea coupling coefficient, the system possesses a unique limit cycle solution, which represents a finite-amplitude, perpetual, interannual oscillation in SST, in upper-ocean heat content, and in equatorial zonal wind. In the phase plane (anomalous SST and thermocline depth), the limit cycle encircles the unstable focal point representing the equilibrium mean state (Fig. 5a). The limit cycle is a stable attractor. Any initial perturbation inside the limit cycle or outside the limit cycle (restricted by the location of the second equilibrium state—an unstable saddle point) will eventually be attracted to the nonlinear periodic solution.

The limit cycle describes intrinsic oscillatory behavior of the coupled ocean–atmosphere. The key feature of the nonlinear oscillation over the eastern equatorial Pacific is that the variation of the thermocline depth leads that of SST by about one-tenth of the oscillation period (Fig. 5b). This feature resembles observed individual ENSO cycles in the 1980s (Fig. 8) and the interannual oscillations simulated by coupled ocean–atmosphere GCMs (e.g., Philander et al. 1992), coupled intermediate models (Zebiak and Cane 1987 and many others), and the hybrid coupled model (Neelin 1990).

The model oscillation results from nonlinear interactions of thermocline displacement and SST variation. The thermocline displacement affects SST by changing the temperature of the water upwelled into the mixed layer, yielding a phase leading of thermocline displacement to SST variation. This phase lead is critical for the turn over from one state of the Southern Oscillation to the other. The SST variation, on the other hand, affects thermocline via changing wind stress and thus the divergence of the upper-ocean currents. This is a slow adjustment process—a delayed response—during which wave dynamics play critical roles. Although the dynamic system model does not explicitly resolve individual wave activity, by considering the basin seesaw mode it implicitly includes collective effects of equatorial Kelvin and Rossby wave and off-equatorial Rossby wave adjustment including processes of boundary reflections. The model oscillation regime occurs when the meridional length scale of the coupled mode is sufficiently large, suggesting that the slow Rossby waves play an overwhelming part.

When the basic state includes annual variations, the limit cycle evolves into a strange attractor if the intensity of the annual variation exceeds a critical amplitude. The corresponding oscillation exhibits deterministic chaos (Fig. 7). This behavior resembles that of the oscillation obtained in the coupled intermediate model of Chang et al. (1995). The primary peak in energy spectrum of the chaotic oscillation (Fig. 7b) is determined by the period of the limit cycle. The subharmonic peaks in the power spectrum result from the asymmetry in the temporal evolution of the limit cycle. It is inferred that an asymmetric 4-year oscillation can induce a sizable quasi-biennial peak. The broadness of the spectral peaks is simply a manifest of the strange attraction of the limit cycle modified by the basic-state annual cycle.

Apparently, ENSO irregularities can be caused by other processes. Considering atmospheric high-frequency stochastic forcing or finer spatial resolution would increase degrees of freedom or raise the order of the dynamic system. Even without annual variation of the basic state, the system could have chaotic oscillations. It is also plausible that, by the same mechanism demonstrated here, the interdecadal variation of the basic state may also cause changes in ENSO evolution as speculated by Wang (1995).

How can a regular annual variation of the basic state cause chaos in the model ENSO cycle? One important cause is that the coupled instability depends on the annually varying basic state. As a result, the warming preferably starts in late boreal spring and peaks in late winter—an ENSO phase-lock to annual cycle (Figs. 9a,b). The regulation of the ENSO phase results in a tendency of period "locking" to an integer multiple of the annual period (Fig. 9c). This, in turn, leads to irregularities in the amplitude and frequency of the oscillation.

Whereas the minimum dynamic system model (3.5a,b) provides a useful conceptual model for understanding the cyclic, chaotic, and phase-locking behavior of ENSO cycle, it involves a number of critical assumptions and simplifications. The most severe limitation of the model arises from its crucial spatial truncation. The east–west seesaw is not a precise description of the thermocline variation. Observations show that the rising of the western Pacific thermocline slightly leads the deepening of the thermocline in the eastern Pacific (Wang 1996, manuscript submitted to *Dyn. Atmos. Oceans*). The Wakata and Sarachik's (1991) work suggests that the node point of the coupled basin mode is located off the equator and to the east of the mid-Pacific basin. The assumption of the equatorial mid-Pacific node point leads to two flaws: the central Pacific thermocline does not vary with time, and the zonally integrated thermocline depth vanishes. Both are at odds with observations. This fails to simulate the eastward propagation of the upper-ocean heat content associated with ENSO, which is evident and primarily confined to the equatorial central Pacific. Similarly, the meridional truncation also severely limits the model's ability in modeling meridional mode interactions. These deficiencies can be eliminated by increasing the degree of freedom of the system. A more realistic model should depict the different meridional

scales of SST and thermocline depth variation and the equatorial phase propagations of the thermocline displacement. These underline the needs for future studies.

Acknowledgments. We thank Steve Zebiak and David Neelin for their insightful comments on an early version of the manuscript. We also thank Feifei Jin and Dennis Moore for enjoyable discussions during the model development and Thomas Schroeder for carefully reading an early version of the manuscript. Thanks are also extended to Mr. R. Wu for drawing Fig. 3 and Mr. Y. Wang for typing formulas. This study has been supported by NOAA GOALS programs under a cooperative agreement, NA37 RJO199. The views expressed herein are those of the author and do not necessarily reflect the view of NOAA or any of its subagencies. This is the School of Ocean and Earth Science and Technology publication number 4110.

APPENDIX A

Equations of Motion in the Coupled Ocean–Atmospheric Model

In the Zebiak and Cane (1987) ocean model, the mixed-layer currents $\mathbf{V}_1$ is expressed as a sum of a vertically mean current of the upper ocean $\mathbf{V}$ and an Ekman flow $\mathbf{V}_e$, which vanishes at the mixed-layer base:

$$\mathbf{V}_1 = \mathbf{V} + \frac{H_2}{H}\mathbf{V}_e, \tag{A.1}$$

where $H_2 = H - H_1$.

The anomalous vertical mean currents, u and v, are depicted by a linear, reduced-gravity model on an equatorial β plane. With long-wave approximation and neglect of meridional wind stress the governing equations are

$$\frac{\partial h}{\partial t} + H\left(\frac{\partial u}{\partial x} + \frac{\partial v}{\partial y}\right) = 0, \tag{A.2a}$$

$$\frac{\partial u}{\partial t} - \beta y v = -g'\frac{\partial h}{\partial x} + lU_a u_a, \tag{A.2b}$$

$$\beta y u = -g'\frac{\partial h}{\partial y}, \tag{A.2c}$$

where u_a and U_a denote, respectively, the zonal component of surface wind and its characteristic scale. In (A.2b), we have linearized the bulk formula for zonal wind stress; thus, the coefficient

$$l \equiv \frac{\rho_a}{\rho_0}\frac{C_D}{H}, \tag{A.3}$$

where ρ_a and ρ_0 are the densities of the surface air and seawater, respectively, and C_D is the drag coefficient.

The Ekman flow $\mathbf{V}_e$ also represents the vertical shear between the mixed layer and subsurface layer and is governed by

$$r_s u_e - \beta y v_e = \frac{H}{H_1} lU_a u_a, \tag{A.4a}$$

$$r_s v_e + \beta y u_e = 0. \tag{A.4b}$$

The vertical velocity at the mixed-layer base is determined by the divergence of mixed layer currents $\mathbf{V}_1$. Using (A.1), (A.2a), and (A.4a,b), it can be shown that near the equator the anomalous upwelling

$$w = H_1\nabla\cdot\mathbf{V} + \frac{H_1H_2}{H}\nabla\cdot\mathbf{V}_e = -\frac{H_1}{H}\frac{\partial h}{\partial t} - H_2\frac{lU_a\beta}{r_s^2}u_a. \tag{A.5}$$

Similarly, the mixed-layer zonal current in the vicinity of the equator is

$$u_1 = u + \frac{H_2}{H}u_e = -\frac{g'}{\beta y}\frac{\partial h}{\partial y} + \frac{H_2}{H_1}\frac{lU_a\beta}{r_s}u_a. \tag{A.6}$$

A thermocline depth anomaly equation can be derived from combining Eqs. (A.2a–c):

$$y^2\frac{\partial h}{\partial t} + \frac{g'H}{\beta^2}\frac{\partial}{\partial t}\left(\frac{2}{y}\frac{\partial h}{\partial y} - \frac{\partial^2 h}{\partial y^2}\right) - \frac{g'H}{\beta}\frac{\partial h}{\partial x} = \frac{lU_aH}{\beta}\left(y\frac{\partial u_a}{\partial y} - u_a\right). \tag{A.7}$$

The atmospheric model is a simplified Lindzen–Nigam (1987) model in which boundary layer winds are taken to be nondivergent. The surface winds u_a and v_a are given by

$$r_a u_a - \beta y v_a = dR\frac{\partial T}{\partial x} \tag{A.8a}$$

$$r_a v_a + \beta y u_a = dR\frac{\partial T}{\partial y}, \tag{A.8b}$$

where r_a is the Rayleigh frictional coefficient, d the atmospheric boundary layer depth normalized by the atmospheric density scale, and R the gas constant.

APPENDIX B

Derivation of Free Wave Solutions

In the absence of wind forcing, the nondimensional thermocline-depth equation (A.7) becomes

$$\frac{\partial}{\partial t}\left[y^2h + \left(\frac{2}{y} - \frac{\partial h}{\partial y} - \frac{\partial^2 h}{\partial y^2}\right)\right] - \frac{\partial h}{\partial x} = 0, \tag{B.1}$$

where y and t are scaled by $(g'H)^{1/4}\beta^{-1/2}$ and $(g'H)^{-1/4}\times\beta^{-1/2}$, respectively. Assume

$$h(x, y, t) = \mathrm{Re}[y\cdot H(y)e^{ik(x-ct)}]. \tag{B.2}$$

The amplitude function $H(y)$ is bounded as $|y| \to \infty$ and satisfies, from (B.1),

$$\frac{d^2H}{dy^2} - \left(\frac{1}{c} + y^2 + \frac{2}{y^2}\right)H = 0. \quad \text{(B.3)}$$

Equation (B.3) has eigen solutions of the following form (Hochstrasser 1965):

$$H_n(y) = e^{-y^2/2}y^{\alpha+1/2}L_n^{(\alpha)}(y^2), \quad \text{(B.4a)}$$

where $L_n^{(\alpha)}(x)$ denotes a generalized Laguerre function

$$L_n^{(\alpha)}(x) = \sum_{k=0}^{n}(-1)^k\binom{n+\alpha}{n-\alpha}\frac{x^k}{k!}, \quad \text{(B.4b)}$$

with

$$\alpha = \pm\frac{3}{2} \quad \text{(B.5)}$$

and

$$c = \begin{cases} -\dfrac{1}{4n+5}\left(\alpha = \dfrac{3}{2}\right), \\ -\dfrac{1}{4n-1}\left(\alpha = -\dfrac{3}{2}\right), \end{cases} \quad n = 0, 1, 2, \cdots. \quad \text{(B.6)}$$

The mode with $\alpha = -3/2$ and $n = 0$ is the Kelvin wave whose phase speed $c = 1$ and meridional structure is $e^{-y^2/2}$. The modes with $\alpha = -3/2$ and $n = 1, 2, \cdots$ are symmetric long Rossby waves whose phase speed

$$c = -\frac{1}{3}, -\frac{1}{7}, -\frac{1}{11}, \cdots \quad \text{(B.7a)}$$

and meridional structures are

$$e^{-y^2/2}L_n^{(-3/2)}(y^2). \quad \text{(B.7b)}$$

The modes with $\alpha = 3/2$ and $n = 0, 1, 2, \cdots$ are antisymmetric long Rossby waves whose phase speed

$$c = -\frac{1}{5}, -\frac{1}{9}, -\frac{1}{13}, \cdots \quad \text{(B.8a)}$$

and meridional structures are

$$e^{y^2/2}y^3L_n^{(3/2)}(y^2). \quad \text{(B.8b)}$$

APPENDIX C

Existence of the Limit Cycle

The existence of linear oscillation requires $b > 0$, $(2a_1 - a_2) > 0$. Define

$$r = [b(2a_1 - a_2)]^{1/2} > 0. \quad \text{(C.1)}$$

Let

$$T' = \frac{b}{r}(2h_E - T_E) \quad \text{(C.2)}$$

$$t' = rt. \quad \text{(C.3)}$$

Substituting (C.2) and (C.3) into the dynamic system (3.5a,b) leads to

$$\frac{dT'}{dt} = -h + dT' + lT'^2 + mT'h + nh^2 \quad \text{(C.4a)}$$

$$\frac{dh}{dt'} = T', \quad \text{(C.4b)}$$

where

$$d = (a_1 + 2b)/r \quad \text{(C.5a)}$$

$$l = -a_3/b, \quad \text{(C.5b)}$$

$$m = (4a_3 - a_4)/r, \quad \text{(C.5c)}$$

$$n = -2b(2a_3 - a_4)/r^2. \quad \text{(C.5d)}$$

According to the theorem of Ye (1965, p. 300), Eqs. (C.4a,b) have one and only one limit cycle solution if

$$dm(l + n) < 0 \quad \text{(C.6)}$$

and

$$|d| \quad \text{is sufficiently small.} \quad \text{(C.7)}$$

REFERENCES

Anderson, D. L. T., and J. P. McCreary, 1985: Slowly propagating disturbances in a coupled ocean–atmosphere model. *J. Atmos. Sci.*, **42,** 615–629.

Balmaseda, M. A., M. K. Davey, and D. L. T. Anderson, 1995: Decadal and seasonal dependence of ENSO prediction skill. *J. Climate,* **8,** 2705–2715.

Battisti, D. S., 1989: On the role of off-equatorial oceanic Rossby waves during ENSO. *J. Phys. Oceanogr.*, **19,** 551–559.

——, and A. C. Hirst, 1989: Interannual variability in the tropical atmosphere–ocean system: Influence of the basic state and ocean geometry. *J. Atmos. Sci.*, **46,** 1687–1712.

Bjerknes, J., 1966: A possible response of the atmospheric Hadley circulation to equatorial anomalies of ocean temperature. *Tellus,* **18,** 820–829.

——, 1969: Atmospheric teleconnections from the equatorial Pacific. *Mon. Wea. Rev.*, **97,** 163–172.

Cane, M. A., 1979: The response of an equatorial ocean to simple wind stress patterns. Part I: Model formulation and analytical results. *J. Mar. Res.*, **37,** 233–252.

——, and D. W. Moore, 1981: A note on low-frequency equatorial basin modes. *J. Phys. Oceanogr.*, **11,** 1578–1584.

——, and S. E. Zebiak, 1985: A theory for El Niño and the Southern Oscillation. *Science,* **228,** 1084–1087.

——, M. Münnich, and S. E. Zebiak, 1990: A study of self-excited oscillations of the tropical ocean–atmosphere system. Part I: Linear analysis. *J. Atmos. Sci.*, **47,** 1562–1577.

Chang, P., B. Wang, T. Li, and L. Ji, 1994: Interactions between the seasonal cycle and ENSO-frequency entrainment and chaos in a coupled atmosphere–ocean model. *Geophys. Res. Lett.*, **21,** 2817–2820.

——, L. Ji, B. Wang, and T. Li, 1995: On the interactions between the seasonal cycle and El Niño–Southern Oscillation in an intermediate coupled ocean–atmosphere model. *J. Atmos. Sci.*, **52,** 2353–2372.

Chao, Y., and S. G. H. Philander, 1993: On the structure of the Southern Oscillation. *J. Climate,* **6,** 450–469.

Gill, A. E., 1980: Some simple solutions for heat-induced tropical circulation. *Quart. J. Roy. Meteor. Soc.*, **106,** 447–462.

——, 1985: Elements of coupled ocean–atmosphere models for the Tropics. *Coupled Ocean–Atmosphere Models,* J. C. J. Nihoul, Ed., Elsevier Oceanography Series, Vol. 40, Elsevier, 303–327.

Graham, N. E., and W. B. White, 1988: The El Niño cycle: A natural oscillator of the Pacific Ocean–atmosphere system. *Science,* **240,** 1293–1302.

Gu, D., and S. G. H. Philander, 1995: Secular changes of annual and interannual variability in the Tropics during the past century. *J. Climate,* **8,** 864–876.

Hirst, A. C., 1986: Unstable and damped equatorial modes in simple coupled ocean–atmosphere models. *J. Atmos. Sci.,* **43,** 606–630.

Hochstrasser, U. W., 1965: Orthogonal polynomials. *Handbook of Mathematical Functions,* M. Abramowitz and I. A. Stegun, Eds., Dover Publications, 1046 pp.

Ji, M., A. Leetmaa, and J. Derber, 1995: An ocean analysis system for seasonal to interannual climate studies. *Mon. Wea. Rev.,* **123,** 460–481.

Jin, F.-F., and J. D. Neelin, 1993a: Modes of interannual tropical ocean–atmosphere interaction—A unified view. Part I: Numerical results. *J. Atmos. Sci.,* **50,** 3477–3503.

——, and ——, 1993b: Modes of interannual tropical ocean–atmosphere interaction—A unified view. Part III: Analytical results in fully coupled cases. *J. Atmos. Sci.,* **50,** 3523–3540.

——, ——, and M. Ghil, 1994: El Niño on the Devil's Staircase: Annual subharmonic steps to chaos. *Science,* **264,** 70–72.

Kessler, W. S., 1991: Can reflected extra-equatorial Rossby waves drive ENSO? *J. Phys. Oceanogr.,* **21,** 444–452.

Latif, M., A. Sterl, E. Maier-Reimer, and M. M. Junge, 1993: Structure and predictability of the El Niño/Southern Oscillation phenomenon in a coupled ocean–atmosphere general circulation model. *J. Climate,* **6,** 700–708.

Lau, K. M., 1981: Oscillations in a simple equatorial climate system. *J. Atmos. Sci.,* **38,** 248–261.

Li, B., and A. J. Clarke, 1994: An examination of some ENSO mechanisms using interannual sea level at the eastern and western equatorial boundaries and the zonally averaged equatorial wind. *J. Phys. Oceanogr.,* **24,** 681–690.

Lindzen, R. S., and S. Nigam, 1987: On the role of sea surface temperature gradients in forcing low level winds and convergence in the Tropics. *J. Atmos. Sci.,* **44,** 2418–2436.

Lorenz, E. N., 1963: Deterministic nonperiodic flow. *J. Atmos. Sci.,* **20,** 130–141.

Mantua, N. J., and D. S. Battisti, 1994: Evidence for the delayed oscillator mechanism for ENSO: The "observed" oceanic Kelvin mode in the far western Pacific. *J. Phys. Oceanogr.,* **24,** 691–699.

——, and ——, 1995: A periodic variability in the Zebiak–Cane coupled ocean–atmospheric model: Air–sea interaction in the western equatorial Pacific. *J. Climate,* **8,** 2897–2927.

Matsuno, T., 1966: Quasi-geostrophic motions in the equatorial area. *J. Meteor. Soc. Japan,* **44,** 25–43.

McCreary, J. P., 1983: A model of tropical ocean–atmosphere interaction. *Mon. Wea. Rev.,* **111,** 370–387.

——, and D. L. T. Anderson, 1984: A simple model of El Niño and the Southern Oscillation. *Mon. Wea. Rev.,* **112,** 934–946.

McWilliams, J. C., and P. R. Gent, 1978: A coupled air and sea model for the tropical Pacific. *J. Atmos. Sci.,* **35,** 962–989.

Munnich, M., M. A. Cane, and S. E. Zebiak, 1991: A study of self-excited oscillations of the tropical ocean–atmosphere system. Part II: Nonlinear cases. *J. Atmos. Sci.,* **48,** 1238–1248.

Murakami, T., and B. Wang, 1993: Annual cycle of equatorial east–west circulation over the Indian and Pacific Oceans. *J. Climate,* **6,** 932–952.

Neelin, J. D., 1989: Interannual oscillations in an ocean GCM-simple atmospheric model. *Philos. Trans. Roy. Soc. London Ser. A,* **329,** 189–205.

——, 1990: A hybrid coupled general circulation model for El Niño studies. *J. Atmos. Sci.,* **47,** 674–693.

——, 1991: The slow sea surface temperature mode and the fast-wave limit: Analytic theory for tropical interannual oscillations and experiments in a hybrid coupled model. *J. Atmos. Sci.,* **48,** 584–606.

——, and F.-F. Jin, 1993: Models of interannual tropical ocean–atmosphere interaction—A unified view. Part II: Analytical results in the weak-coupling limit. *J. Atmos. Sci.,* **50,** 3504–3522.

——, M. Latif, and F.-F. Jin, 1994: Dynamics of coupled ocean–atmosphere models: The tropical Problem. *Annu. Rev. Fluid Mech.,* **26,** 617–659.

Philander, S. G. H., 1990: *El Niño, La Niña, and the Southern Oscillation.* Academic Press, 293 pp.

——, T. Yamagata, and R. C. Pacanowski, 1984: Unstable air–sea interaction in the Tropics. *J. Atmos. Sci.,* **41,** 604–613.

——, N. C. Lau, R. C. Pacanowski, and M. J. Nath, 1989: Two different simulations of Southern Oscillation and El Niño with coupled ocean–atmosphere general circulation models. *Philos. Trans. Roy. Soc. London Ser. A,* **329,** 167–178.

——, R. C. Pacanowski, N. C. Lau, and M. J. Nath, 1992: Simulation of ENSO with a global atmospheric GCM coupled to a high-resolution, tropical Pacific ocean GCM. *J. Climate,* **5,** 308–329.

Rasmusson, E. M., and T. H. Carpenter, 1982: Variations in tropical sea surface temperature and surface wind fields associated with the Southern Oscillation/El Niño. *Mon. Wea. Rev.,* **110,** 354–384.

Schneider, E. D., B. Huang, and J. Shukla, 1995: Ocean wave dynamics and El Niño. *J. Climate,* **8,** 2415–2439.

Schopf, P. S., and M. J. Suarez, 1988: Vacillations in a coupled ocean–atmosphere model. *J. Atmos. Sci.,* **45,** 549–566.

——, and ——, 1990: Ocean wave dynamics and the time scale of ENSO. *J. Phys. Oceanogr.,* **20,** 629–645.

Suarez, M. J., and P. S. Schopf, 1988: A delayed action oscillator for ENSO. *J. Atmos. Sci.,* **45,** 3283–3287.

Sverdrup, H. U., 1947: Wind-driven currents in a baroclinic ocean with application to the equatorial currents of the eastern Pacific. *Proc. Nat. Acad. Sci. USA,* **33,** 318–326.

Trenberth, K. E., and D. J. Shea, 1987: On the evolution of the Southern Oscillation. *Mon. Wea. Rev.,* **115,** 3078–3096.

Tziperman, E., L. Stone, M. Cane, and H. Jarosh, 1994: El Niño chaos: Overlapping of resonances between the seasonal cycle and the Pacific Ocean–atmosphere oscillator. *Science,* **264,** 72–74.

——, M. A. Cane, and S. E. Zebiak, 1995: Irregularity and locking to the seasonal cycle in an ENSO predication model as explained by quasi-periodicity route to chaos. *J. Atmos. Sci.,* **52,** 293–306.

Vallis, G. K., 1988: Conceptual models of El Niño and the Southern Oscillations. *J. Geophys. Res.,* **93**(C), 13 979–13 991.

Wakata, Y., and E. S. Sarachik, 1991: Unstable coupled atmosphere–ocean basin modes in the presence of a spatially varying basic state. *J. Atmos. Sci.,* **48,** 2060–2077.

Wang, B., 1995: Interdecadal changes in El Niño onset in the last four decades. *J. Climate,* **8,** 267–285.

——, and Y. Wang, 1996: Temporal structure of the Southern Oscillation as revealed by waveform and wavelet analysis. *J. Climate,* **9,** 1586–1598.

——, T. Li, and P. Chang, 1995: An intermediate model of the tropical Pacific Ocean. *J. Phys. Oceanogr.,* **25,** 1599–1616.

Wang, C., and R. H. Weisberg, 1994: On the "slow mode" mechanism in ENSO-related coupled ocean–atmosphere models. *J. Climate,* **7,** 1657–1667.

Webster, J. P., and S. Yang, 1992: Monsoon and ENSO: Selectively interactive system. *Quart. J. Roy. Meteor. Soc.,* **118,** 877–926.

Wyrtki, K., 1975: El Niño—The dynamic response of the equatorial Pacific Ocean to atmospheric forcing. *J. Phys. Oceanogr.,* **5,** 572–584.

Xie, S.-P., A. Kubikawa, and K. Hanawa, 1989: Oscillations with two feedback processes in a coupled ocean–atmosphere model. *J. Climate,* **2,** 946–964.

Yamagata, T., 1985: Stability of a simple air–sea coupled model in the Tropics. *Coupled Ocean–Atmosphere Models,* J. C. J. Nihoul, Ed., Elsevier Oceanography Series, Vol. 40, Elsevier, 637–657.

Ye, Y. Q., 1965: *Theory of Limit Cycle* (in Chinese). Science and Technology Press, 369 pp.

Zebiak, S. E., and M. A. Cane, 1987: A model El Niño–Southern Oscillation. *Mon. Wea. Rev.,* **115,** 2262–2278.